Intermetallics as Zintl Phases: $Yb_2Ga_4Ge_6$ and $RE_3Ga_4Ge_6$ (RE = Yb, Eu): Structural Response of a $[Ga_4Ge_6]^{4-}$ Framework to Reduction by Two Electrons

Marina A. Zhuravleva,[a] James Salvador,[a] Daniel Bilc,[b] Subhendra D. Mahanti,[b] John Ireland,[c] Carl R. Kannewurf,[c] and Mercouri G. Kanatzidis*[a]

Abstract: Two new intermetallic compounds, $Yb_2Ga_4Ge_6$ and $Yb_3Ga_4Ge_6$, were obtained from reactions in molten Ga. A third compound, $Eu_3Ga_4Ge_6$, was produced by direct combination of the elements. The crystal structures of these compounds were studied by single-crystal X-ray diffraction. $Yb_2Ga_4Ge_6$ crystallizes in an orthorhombic cell with $a = 4.1698(7)$, $b = 23.254(4)$, $c = 10.7299(18)$ Å in the polar space group $Cmc2_1$. The structure of $RE_3Ga_4Ge_6$ is monoclinic, space group $C2/m$, with cell parameters $a = 23.941(6)$, $b = 4.1928(11)$, $c = 10.918(3)$ Å, $\beta = 91.426(4)°$ for RE = Yb, and $a = 24.136(2)$, $b = 4.3118(4)$, $c = 11.017(1)$ Å, $\beta = 91.683(2)°$ for RE = Eu. The refinement [$I > 2\sigma(I)$] converged to the final residuals $R_1/wR_2 = 0.0229/0.0589$, 0.0411/0.1114, and 0.0342/0.0786 for $Yb_2Ga_4Ge_6$, $Yb_3Ga_4Ge_6$, and $Eu_3Ga_4Ge_6$, respectively. The structures of these two families of compounds can be described by a Zintl concept of bonding, in which the three-dimensional $[Ga_4Ge_6]^{n-}$ framework serves as a host and electron sink for the electropositive RE atoms. The structural relation of $RE_3Ga_4Ge_6$ to of $Yb_2Ga_4Ge_6$ lies in a monoclinic distortion of the orthorhombic cell of $Yb_2Ga_4Ge_6$ and reduction of the $[Ga_4Ge_6]$ network by two electrons per formula unit. The results of theoretical calculations of the electronic structure, electrical transport data, and thermochemical and magnetic measurements are also reported.

Keywords: flux synthesis · gallium · germanium · lanthanides · Zintl phases

Introduction

The Ga-flux synthetic technique has proven successful not only for the synthesis of novel intermetallics, but also for the discovery of new rare earth (RE) and Group 13/14 Zintl phases. We have reported a number of intermetallics grown from Ga flux; these include $RENiSi_3$,[1] Sm_2NiGa_{12},[2] $RE_4FeGa_{12-x}Ge_x$,[3] $RE_{0.67}M_2Ga_{5+n-x}Ge_x$[4] (M = Ni, Co), RE_3Ga_9Ge,[5] $REMGa_3Ge$ (M = Ni, Co), and $RE_3Ni_3Ga_8Ge_3$.[6,7] However, examples of Zintl compounds obtained from molten Ga are relatively scarce and include the clathrate compounds $M_8Ga_{16}Tt_{30}$[8,9] (M = Ba, Sr; Tt = Si, Ge) and the Zintl phase $Eu_4Ga_8Ge_{16}$.[10] The record of Yb and Eu Zintl phases with a transition metal and a pnictide Pn is quite extensive. It includes $Yb_{14}MSb_{11}$ (M = Mn,[11] Zn[12]), $Eu_{14}MnPn_{11}$[13] and $Eu_{13}AMnSb_{11}$[14] (A = Ca, Sr, Ba, Yb) compounds of the so-called 14-1-11 family,[15] $Eu_{10}Mn_6Sb_{13}$,[16] $Yb_9Zn_4Bi_9$,[17] and $EuFe_4Sb_{12}$.[18] Various binary and ternary Yb and Eu Zintl compounds with Group 14 and/or Group 15 elements such as $Eu_{16}Pn_{11}$ and $Yb_{16}Pn_{11}$ (Pn = Sb, Bi),[19,20] Eu_2Si,[21] Eu_5Si_3 and Yb_3Si_5,[22] $Yb_{36}Sn_{23}$,[23] $Yb_{31}Pb_{20}$,[24] and $EuSn_3Sb_4$,[25] have also been reported. Numerous examples of equiatomic EuTX[26] and YbTAl[24] compounds (T = transition metal, X = Group 13, 14, or 15 element) have been described. Zintl phases combining Eu(Yb) and Group 13 and 14 elements are more rare. They include the above-mentioned $Eu_4Ga_8Ge_{16}$, $EuGa_{2\pm x}Ge_{4\pm x}$[27] and EuInGe.[28]

Recently, we described a new, electrically conductive, nonoxidic material, namely, YbGaGe, which exhibits zero thermal expansion between 100 and 300 K by means of an electronic mechanism.[29] YbGaGe is unique in exhibiting zero thermal expansion; its isostructural analogue YbGaSn

[a] M. A. Zhuravleva, J. Salvador, M. G. Kanatzidis
Department of Chemistry
Michigan State University
East Lansing, MI, 48824 (USA)
Fax: (+1) 517-353-1793
E-mail: Kanatzidis@chemistry.msu.edu

[b] D. Bilc, S. D. Mahanti
Department of Physics and Astronomy
Michigan State University
East Lansing, MI, 48824 (USA)

[c] J. Ireland, C. R. Kannewurf
Department of Electrical Engineering and Computer Science
Northwestern University, Evanston, IL 60208 (USA)

 DOI: 10.1002/chem.200305755

displays normal positive thermal-expansion properties. Here we present additional chemistry of the Yb–Ga–Ge system, which apparently is chemically rich. We describe two related Zintl compounds: $Yb_2Ga_4Ge_6$ and $RE_3Ga_4Ge_6$ (RE = Yb, Eu). They contain the $[Ga_4Ge_6]^{4-(6-)}$ framework and are an interesting example of the power of the Zintl concept in describing how the observed framework structures respond when two electrons are added or removed.

Results and Discussion

Synthesis: $Yb_2Ga_4Ge_6$ (**1**) and $Yb_3Ga_4Ge_6$ (**2**) were first obtained from Yb/Ni/Ga/Ge reactions in liquid Ga, from which the hexagonal phase $Yb_{0.67}Ni_2Ga_{6-x}Ge_x$[30,4] ($x \approx 0.67$) was isolated in high yield, whereas **1** and **2** were present in only minor quantities. Nevertheless, the formation of **1** and **2** at reaction stoichiometries far from their ideal compositions suggested high stability of their crystal structures. Consequently, we conducted reactions in the absence of Ni and with the appropriate Yb:Ge ratio, and these led to **2** as a pure phase in high yield. Thus far three phases are known to form in the Yb/Ga/Ge system under Ga-flux conditions: the Zintl phases **1** and **2** reported herein, and the metallic compound Yb_3Ga_9Ge.[5] The lattice parameters[31] and the stability regions of these three compounds were found to be closely interrelated. Despite their close relationship, however, these phases are typically observed in pure form, rather than as multiphase mixtures. Scanning electrom micrographs of typical crystals of **1** and **2** grown under Ga-flux conditions are shown in Figure 1.

The range of stability of **2** is quite broad; this phase is the product of the Ga-flux reactions conducted at higher temperatures, in particular those involving a short isothermal step at 1000 °C and long isothermal step at 850 °C. Under such conditions, the single phase of **2** was obtained at Yb:Ge ratios[32] of 1:3 or 1:2. At a Yb:Ge ratio of 1:1, orthorhombic Yb_3Ga_9Ge was produced in pure form. The Yb analogue of **2** ($Yb_3Ga_4Ge_6$) could also be produced by direct combination of the elements. The Eu analogue of **2** ($Eu_3Ga_4Ge_6$) was thus far obtained only by direct-combination reactions. Numerous attempts to synthesize $Eu_3Ga_4Ge_6$ by using Ga flux were largely unsuccessful and led primarily to the Zintl phase $Eu_4Ga_8Ge_{16}$.[10]

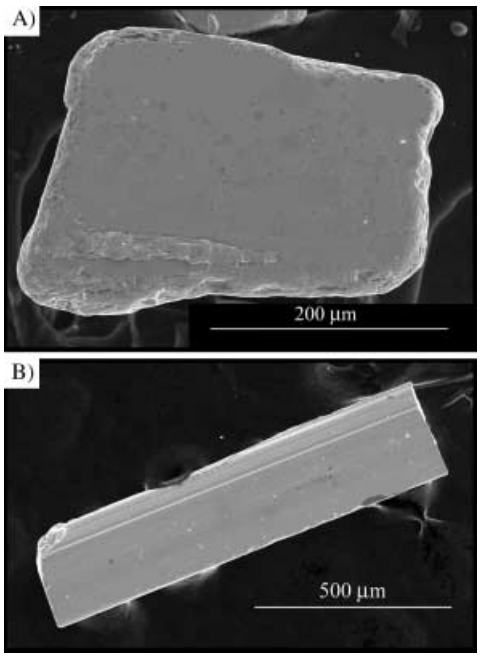

Figure 1. SEM photograph of typical Ga-flux grown crystals. A) $Yb_2Ga_4Ge_6$ (**1**); B) $Yb_3Ga_4Ge_6$ (**2**).

The stability range of **1** is very narrow; the Ga-flux synthesis of **1** requires lower temperatures than that used for growth of **2**. For instance, the formation of **1** was only observed at temperatures no higher than 800 °C. At even lower temperatures (750 °C and 700 °C) the Yb_3Ga_9Ge phase became favorable and formed as a single phase.

Differential thermal analysis (DTA) of **1** show that it is stable (in vacuo) and does not undergo any melting or decomposition up to 1000 °C. The DTA of **2** indicates that $Yb_3Ga_4Ge_6$ ($Eu_3Ga_4Ge_6$) melt congruently at 670 °C (660 °C) and recrystallize at 630 °C (640 °C). Powder X-ray diffraction patterns taken prior to and after the DTA measurements revealed no changes in phase composition. Neither interconversion of phases **1** and **2** nor transformation to the related phases Yb_3Ga_9Ge and $Eu_4Ga_8Ge_{16}$ was observed.

Structure refinement of 1: The first unit cell reduction in SMART[47] initially gave a *C*-centered monoclinic lattice with parameters $a = 23.257(4)$, $b = 4.1699(7)$, $c = 10.744(1)$ Å and β very close to 90° ($\beta = 90.07(1)°$). However, subsequent cell determinations using a larger number of frames (total of ca. 1000) yielded an orthorhombic *C*-centered lattice with cell parameters $a = 4.1732(6)$, $b = 23.276(3)$, $c = 10.738(2)$ Å. The systematic absences led to three possible space groups: $Cmc2_1$ (no. 36), *Cmcm* (no. 63), and *Ama*2 (no. 40). The mean $|E^{2-}-1|$ value of 0.666 pointed to the possibility of a noncentrosymetric space group.[33] The combined figure of merit (CFOM) also favored the choice of noncentrosymmetric space groups $Cmc2_1$ and *Ama*2; of these $Cmc2_1$ had the lowest CFOM value (1.82 %). Thus, the $Cmc2_1$ space group was chosen for the structure solution and found to be correct during structure refinement. Attempts to solve and refine the structure in the centrosymmetric space group *Cmcm* were also made, but led to an extremely poor convergence (ca. 50 %) of the calculated versus observed structure factors; this confirms the correctness of the structure solution in $Cmc2_1$.

Crystal structure of $Yb_2Ga_4Ge_6$ (1): The polar, noncentrosymmetric $[Ga_4Ge_6]^{4-}$ network is shown in Figure 2; the Yb atoms lie in the tunnels of the network. The tunnels in $[Ga_4Ge_6]^{4-}$ have various shapes and sizes that can be characterized by the shape of their cross sections. The smaller tunnels are vacant and have cross sections consisting of three-, five-, and six-membered rings, whereas wider tunnels with seven- and nine-membered rings are occupied by Yb(2) and Yb(1) atoms, respectively.

The three-dimensional (3D) $[Ga_4Ge_6]$ framework is made up of four-coordinate atoms and conforms to the require-

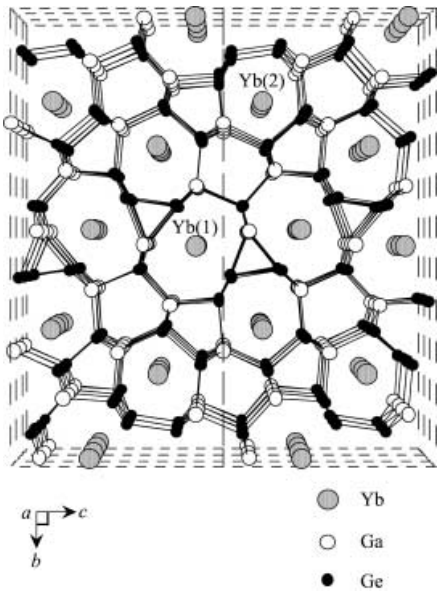

Figure 2. The noncentrosymmetric structure of $Yb_2Ga_4Ge_6$ (**1**) viewed down the *a* axis. Two Yb sites are labeled. The dashed lines indicate the unit cell (two unit cells are shown).

ments of the Zintl concept. According the octet rule, the framework is electron-deficient, as each Ga atom has four neighbors, but only three electrons are available for bonding (see below for Ga and Ge coordination environments). The one extra electron per Ga atom (a total of four per formula unit) is donated by the electropositive Yb atoms, which are expected to be in a 2+ oxidation state (supported by the magnetic susceptibility data reported below). The charge balanced formula of **1** is thus $[Yb_2]^{4+}[Ga_4Ge_6]^{4-}$.

The local coordination polyhedra of Ge and Ga atoms (within the limiting sphere of 3 Å) and Yb atoms (within 3.5 Å) are shown in Figure 3. All Ga and Ge atoms are four-coordinate and have almost tetrahedral geometries (Figure 3 A). For the Ge(3) and Ge(6) atoms, the angles only slightly diverge from those of an ideal tetrahedron [108.07(5)–114.07(7)° for Ge(3), and 103.31(5)–114.82(7)° for Ge(6)]. The Ge(1)- and Ge(4)-centered tetrahedra are moderately distorted [90.59(6)–118.11(4)° for Ge(1), and 100.60(5)–125.86(7)° for Ge(4)]. The remaining two Ge atoms have grossly distorted environments with angles that range from 58.82(5) to 124.38(4)° for Ge(2), and from 60.89(6) to 123.55(4)° for Ge(5). The average Ge–Ge distance in **1** is 2.54 Å; in view of the sum of covalent radii[34] for two Ge atoms (2.44 Å) it can be considered normal. It is also similar to the Ge–Ge distances found in elemental Ge[35] (2.45 Å).

The immediate coordination spheres of Ga atoms contain only Ge atoms (Figure 3 B). The Ga(1)-, Ga(2)-, and Ga(4)-centered tetrahedra are only slightly distorted. The Ge-Ga-Ge angles vary from 102.34(5) to 119.90(7)° for Ga(1), from 100.81(5) to 127.40(7)° for Ga(2), and from 102.85(5) to 115.43(4)° for Ga(4). However, the tetrahedron formed around Ga(3) is strongly compressed; one of the angles is as

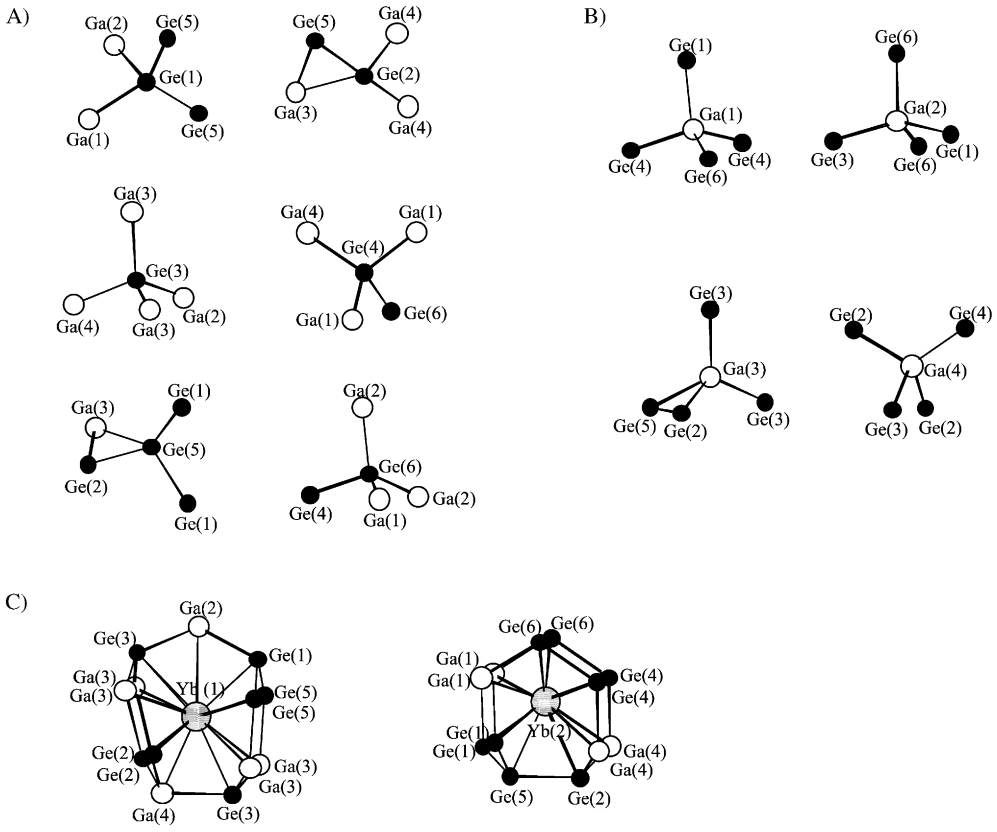

Figure 3. The local coordination environments of A) Ge atoms, B) Ga atoms, and C) Yb atoms in the structure of **1**.

small as 60.30(5)°. The average Ga–Ge distance in **1** is quite short, about 2.51 Å. Compared to the sum of singly bonded metallic radius for Ga[34] and covalent radius for Ge[35] (2.47 Å), the Ga–Ge interactions are certainly strongly bonding. Thus, from the connectivity data we could conclude that the rigidity of the $[Ga_4Ge_6]$ network is primarily due to the strong Ga–Ge interactions, although the Ge–Ge interactions are also quite strong.

The nearest-neighbor coordination environments of Yb atoms are shown in Figure 3C. The Yb(1) atom is located in the center of a cage consisting of thirteen Ga and Ge atoms. The Yb(2) atom has twelve Ga and Ge neighbors in its immediate coordination sphere. The connectivity between the Yb atoms and the framework is also strongly bonding. Thus, the Yb–Ga bond lengths in **1** vary from 3.0957(15) to 3.4882(13) Å, and Yb–Ge distances range from 3.0567(14) to 3.3445(11) Å. The average Yb–Ge and Yb–Ga distances in **1** are 3.15 and 3.34 Å, respectively. Considering the sum of single-bonded metallic radii (coordination number 12 for Yb^{II} is considered) for Yb and Ge (3.15 Å) and Yb and Ga (3.18 Å), these interactions are quite strong and have a considerable covalent contribution to the bonding character.

Interestingly, in the related Zintl compound $Eu_4Ga_8Ge_{16}$,[10] the Eu atoms are located in much larger cages with corresponding Eu–Ga and Eu–Ge contacts ranging between 3.37 and 3.58 Å, respectively. The Eu atoms seem to be "rattling" in the cages, as suggested by the enlarged displacement parameters of Eu atoms and lower thermal conductivity of this material. However, in **1**, no "rattling" or any abnormality in the displacement ellipsoids was observed (see Table 3). Thus, the Yb atoms can not be regarded as being merely "guests" in a host $[Ga_4Ge_6]$ framework, but evidently participate in covalent bonding with it.

Structure refinement of $RE_3Ga_4Ge_6$ (2; RE = Yb, Eu): For $Yb_3Ga_4Ge_6$, the initial cell suggested by the program was a monoclinic *C*-centered cell with a volume eight times larger than that of the true structure (cell parameters $a = 47.948(6)$, $b = 8.4025(9)$, $c = 21.892(4)$ Å, $\beta = 91.41(1)°$). The cell enlargement was most likely caused by the $\lambda/2$ radiation problem. Further cell reductions yielded a correct cell with parameters $a = 23.941(6)$, $b = 4.1928(11)$, $c = 10.918(3)$ Å, $\beta = 91.426(4)°$, which was then used for data integration and structure solution. The monoclinic space group *C*2/*m* was chosen and was found to be correct during structure refinement. The final convergence factor of $R_1 = 0.0426$ was obtained on correcting for secondary extinction and refining all atoms anisotropically. However, additional reduction of the *R* value to 0.0411 was possible by introducing a twinning law (matrix 001, 0–10, 100) that accounted for twofold rotational twinning about the *b* axis. This particular type of twinning is likely to occur in monoclinic systems with β close to 90°. For $Eu_3Ga_4Ge_6$, initial indexing of the reflections readily gave the correct monoclinic *C*-centered lattice with $a = 24.136(2)$, $b = 4.3118(4)$, $c = 11.017(1)$ Å, $\beta = 91.683(2)°$, which was further used for intensity integration. Structural refinement in *C*2/*m* resulted in a final convergence of $R_1 = 3.42\%$ (on applying a secondary extinction coefficient and refining all atoms anisotropically). No further reduction in *R* values was observed after application of the twinning law that was successfully used in the case of $Yb_3Ga_4Ge_6$.

Crystal structure of $RE_3Ga_4Ge_6$ (2; RE = Yb, Eu): The structure of **2** (RE = Yb) is presented in Figure 4. For consistency, the Yb, Ga, and Ge atoms in the 3D $[Ga_4Ge_6]$ framework are depicted in the same way as for **1**. The Ga–Ge

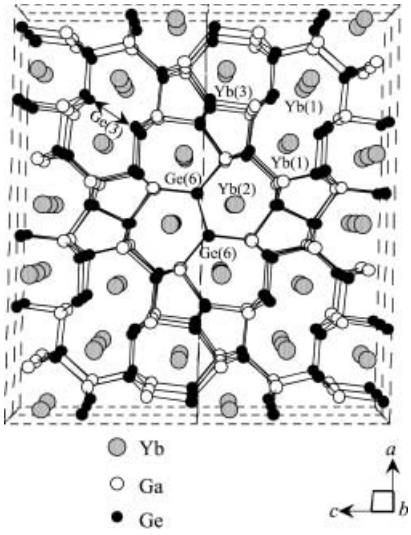

Figure 4. The structure of $Yb_3Ga_4Ge_6$ (**2**) projected onto the *ac* plane. Three crystallographically different Yb sites are marked. Three-coordinate Ge atoms (Ge(3) and Ge(6)) are also labeled. The unit cell is shown in dashed lines.

frameworks in **1** and **2** differ in the number of electrons, that is, $[Ga_4Ge_6]^{4-}$ versus $[Ga_4Ge_6]^{6-}$. The tunnels formed by the framework in **2** are quite different from those found in **1**. The only unfilled tunnels are five-membered. The remaining tunnels are wider and occupied by Yb atoms. A pair of Yb(1) atoms (Yb(1)–Yb(1) 4.271 Å) resides in a large ten-membered tunnel. Additionally, there are two types of seven-membered channels, one of which hosts Yb(2) and the other Yb(3) atoms.

In contrast to **1**, the $[Ga_4Ge_6]$ 3D framework in **2** consists of both four- and three-coordinate Ge atoms. Formally, **2** is a chemically reduced (by two electrons) version of **1**. This can be understood by the addition of two electrons, which turns the framework into a new arrangement that contains both four- and three-coordinate atoms. The bonding in **2** can still be explained within the Zintl concept. First, the Yb (Eu) atoms are in the +2 oxidation state, as suggested by magnetic susceptibility data (see below). The position of the Yb peaks (below the Fermi level) in the calculated density of states of Yb atoms in **2** also points to Yb^{2+} as opposed to Yb^{3+} (see below). Thus, the possibility of Yb (Eu) existing in the +3 state in **2** can be ruled out.

The assignment of the charge distribution to the remaining ten Ga and Ge atoms was done according the octet rule as follows: All of the Ga atoms are located at the four-coordinate sites, and therefore a charge of −1 was assigned to each of them to complete the octet. Zero charge was assigned to the four Ge atoms in the tetrahedral environ-

ments, and a charge of −1 to the remaining two Ge atoms with three-coordinate (trigonal-planar and pyramidal) environments. The resulting charge-balanced formula is $[Yb_3]^{6+}[Ga_4^{4-}Ge_4^{0}Ge_2^{2-}]$. The ambiguous sites containing three-coordinate atoms were especially carefully scrutinized: first, by means of bonding considerations and then with calculations of the electronic band structure by way of minimization of the energy of the system, as described in the Experimental Section. The occurrence of a Ga^{2-} instead of Ge^{-} on the three-coordinate sites is less likely from the chemical standpoint given the higher electronegativity of Ge.

The local coordination environments of Ga, Ge and Yb atoms in **2** are shown in Figure 5. The environment of all Ga atoms within 3.0 Å is tetrahedral (Figure 5 A). The departure from ideal tetrahedral angles is not substantial: 102.23(6)–123.24(8)° for Ga(1), 91.71(7)–113.84(8)° for Ga(2), 93.66(6)–117.51(5)° for Ga(3), and 99.87(6)–117.38(5)° for Ga(4). The Ga–Ge bond lengths range from 2.501(2) to 2.617(2) Å with an average Ga–Ge distance of 2.54 Å, comparable to that observed in **1** (2.51 Å). The average Ge–Ge bond length in **2** is 2.50 Å, and thus this bond is even stronger than that found in **1** (2.54 Å). Thus, the $[Ga_4Ge_6]$ framework in **2** is an extremely robust unit, held together by strong Ga–Ge and Ge–Ge interactions.

The Ge coordination environments that contain only the Ga and Ge neighbors (Yb atoms were excluded for clarity) are shown in Figure 5 B. Here, the Ge(1), Ge(2), Ge(4), and Ge(5) atoms are four-coordinate, whereas Ge(3) and Ge(6) are three-coordinate. Within the four-coordinate environment of Ge atoms, the angles are close to those of an ideal tetrahedron: 99.02(7)–119.49(5)° for Ge(1), 99.86(8)–132.92(8)° for Ge(2), 102.56(6)–126.32(8)° for Ge(4), and 107.22(7)–112.31(8)° for Ge(5). The Ge(3) atom is in the apex position of a distorted trigonal pyramid with a base of two Ga(2) atoms and one Ge(5) atom. The corresponding Ge(5)-Ge(3)-Ga(2) and Ga(2)-Ge(3)-Ga(2) angles are 109.66(5)° and 113.84(8)°, respectively. The Ge(6) atom lies in a trigonal-planar environment of Ga(3), Ga(4), and Ge(6). The angles only vary slightly from truly trigonal (112.31(8), 112.78(9), and 124.88(10)°). The plane of a Ge(6)-centered triangle is perpendicular to the *b* axis.

The immediate coordination spheres of Yb atoms within a radius of 3.6 Å are depicted in Figure 5 C. The Yb(1) and Yb(2) atoms have twelve Ga and Ge neighbors, while Yb(3) has thirteen. Interestingly, some of the Yb–Ge bonding contacts are as short as 2.9321(17) Å, as is the case for Yb(1)–Ge(3). The average Yb–Ge bond length in **2** of 3.15 Å (identical to that found in **1**) suggests that the bonding interactions between Yb and Ge are very strong. The average Yb–Ga distance in **2** is 3.33 Å, which again is in the bonding realm and very close to that found in **1** (3.34 Å). The relatively strong Yb–Ga/Ge network interactions are also responsible for the stability of these phases to moisture and air. This is in contrast to classical Zintl phases containing alkaline-earth metals, for example, which tend to be air-sensitive.

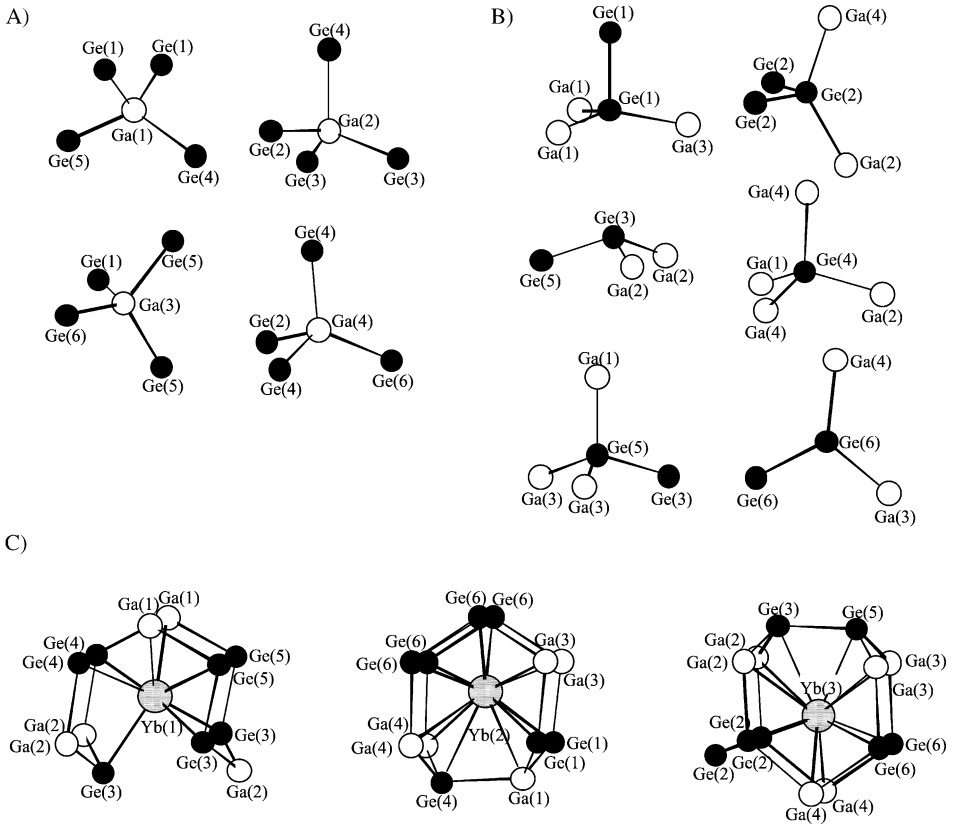

Figure 5. The local coordination environments of A) Ga atoms, B) Ge atoms, and C) Yb atoms in the structure of **2**.

Information on the data collection and structure refinement of **1** and **2** is given in Tables 1 and 2, respectively. The final atomic positions and equivalent atomic displacement parameters for **1** are listed in Table 3; selected interatomic distances (up to 3.5 Å) are presented in Table 4. For **2**, the final atomic positions and equivalent atomic displacement parameters are given in Table 5, and the selected interatomic distances (up to 3.5 Å) for $Yb_3Ga_4Ge_6$ are presented in Table 6. Complete crystallographic information for **1** and **2** can be found in the Supporting Information.

Ga/Ge assignment in 1 and 2: Because of very similar X-ray scattering lengths of Ga and Ge atoms, the assignment of their positions in the structure is very difficult. In our previous studies, we used the observed connectivity in the struc-

Table 1. Crystal data and structure refinement for $Yb_2Ga_4Ge_6$ (**1**).

empirical formula	$Yb_2Ga_4Ge_6$
formula weight	1060.50
temperature [K]	298(2)
wavelength [Å]	0.71073
crystal system	orthorhombic
space group	$Cmc2_1$ (no. 36)
a [Å]	4.1698(7)
b [Å]	23.254(4)
c [Å]	10.7299(18)
V [Å^3]	1040.4(3)
Z	4
ρ_{calcd} [g cm^{-3}]	6.770
absorption coefficient [mm^{-1}]	44.936
F(000)	1824
crystal size [mm]	0.12×0.1×0.08
θ range for data collection [°]	2.58–29.16
index ranges	$-5\le h\le 5$, $-31\le k\le 30$, $-14\le l\le 14$
reflections collected	5431
independent reflections	1479 ($R_{int}=0.0395$)
completeness to θ	96.8 %
refinement method	full-matrix least-squares on F^2
data/restraints/parameters	1479/1/74
goodness of fit on F^2	1.109
final R indices $[I>2\sigma(I)]$[a]	$R_1=0.0229$, $wR_2=0.0589$
R indices (all data)	$R_1=0.0234$, $wR_2=0.0591$
absolute structure parameter (Flack)	−0.03(3)
extinction coefficient	0.00047(5)
largest diff. peak/hole [e Å^{-3}]	1.452/−1.315

[a] $R_1=\Sigma\,||F_o|-|F_c||/\Sigma|F_o|$; $wR_2=[\Sigma w\{|F_o|-|F_c|\}^2/\Sigma w|F_o|^2]^{1/2}$.

Table 2. Crystal data and structure refinement for $RE_3Ga_4Ge_6$ (**2**) (RE = Yb, Eu).

empirical formula	$Yb_3Ga_4Ge_6$	$Eu_3Ga_4Ge_6$
formula weight	1233.54	1168.63
T [K]	298(2)	298(2)
wavelength [Å]	0.71073	0.71073
Crystal system	monoclinic	monoclinic
space group	$C2/m$ (no. 12)	$C2/m$ (no. 12)
a [Å]	23.941(6)	24.136(2)
b [Å]	4.193(1)	4.3118(4)
β [°]	91.426(4)	91.683(2)
c [Å]	10.918(3)	11.017(1)
V [Å^3]	1095.6(5)	1146.0(2)
Z	4	4
ρ_{calcd} [g cm^{-3}]	7.478	6.783
absorption coefficient [mm^{-1}]	51.107	40.795
F(000)	2104	2020
crystal size [mm]	0.06×0.08 × 0.30	0.2× 0.05 × 0.05
θ range for data collection [°]	1.70 to 28.37	1.69 to 26.99
index ranges	$-27\le h\le 30$, $-5\le k\le 5$, $-13\le l\le 13$	$-30\le h\le 26$, $-5\le k\le 5$, $-14\le l\le 14$
reflections collected	4673	4250
independent reflections	1412 ($R_{int}=0.0447$)	1429 ($R_{int}=0.0412$)
completeness to θ	90.5 %	100 %
refinement method	full-matrix least-squares on F^2	full-matrix least-squares on F^2
data/restraints/parameters	1412/0/81	1429/1/80
goodness of fit on F^2	1.095	1.042
final R indices $[I>2\sigma(I)]$[a]	$R_1=0.0411$, $wR_2=0.1114$	$R_1=0.0342$, $wR_2=0.0786$
R indices (all data)	$R_1=0.0425$, $wR_2=0.1129$	$R_1=0.0482$, $wR_2=0.0824$
extinction coefficient	0.00065(8)	0.00113(7)
largest diff. peak/hole [e Å^{-3}]	3.118/−2.778	3.297/−2.245

[a] $R_1=\Sigma\,||F_o|-|F_c||/\Sigma|F_o|$; $wR_2=[\Sigma w\{|F_o|-|F_c|\}^2/\Sigma w|F_o|^2]^{1/2}$.

Table 3. Atomic coordinates and equivalent isotropic displacement parameters[a] [Å$^2\times10^3$] for $Yb_2Ga_4Ge_6$ (**1**).

Atomic position	Wyckoff symbol	x	y	z	U(eq)
Yb(1)	4*a*	0	0.0187(1)	0.1308(1)	14(1)
Yb(2)	4a	0	0.3006(1)	0.3130(1)	14(1)
Ge(1)	4a	0	0.1411(1)	0.0213(1)	13(1)
Ge(2)	4a	0	0.4285(1)	0.2255(1)	11(1)
Ge(3)	4a	0	0.0709(1)	0.4079(1)	12(1)
Ge(4)	4a	0	0.2226(1)	0.6074(1)	12(1)
Ge(5)	4a	0	0.4124(1)	0.4626(1)	12(1)
Ge(6)	4a	0	0.7049(1)	0.2878(1)	12(1)
Ga(1)	4a	0	0.2501(1)	−0.0002(2)	11(1)
Ga(2)	4a	0	0.1497(1)	0.2540(1)	11(1)
Ga(3)	4*a*	0	0.5143(1)	0.3790(1)	14(1)
Ga(4)	4a	0	0.1144(1)	0.6287(1)	13(1)

[a] U(eq) is defined as one-third of the trace of the orthogonalized U^{ij} tensor.

ture, coupled with thorough elemental analysis, in assigning Ga/Ge and Al/Si from X-ray data. In some instances, this approach was further validated by additional neutron[36] crystallographic studies.[6,37,38] The issue of Ga/Ge distribution in **1** and the Yb version of **2** was approached as follows.[39] First, careful elemental analysis on crystalline samples of **1** and **2** indicated a higher content of Ge than of Ga. This fixes the composition at $Yb_2Ga_4Ge_6$ and $Yb_3Ga_4Ge_6$. Second, since the covalent radius of Ge is slightly, but discernibly, smaller than that of Ga, the shorter Yb–M distances were assigned to Yb–Ge, and the longer ones to Yb–Ga interactions. This narrowed down the number of possibilities to two or three. Using the assignments made above, we generated two models for each compound in which 1) the shortest homoatomic distances were ascribed to Ge–Ge and the longer ones to Ga–Ga, and 2) the distribution of Ga and Ge throughout the structure was even. For compound **1**, the structural refinement immediately yielded a better convergence factor (0.0229 versus 0.0233) for model 2. For **2**, the convergence factor remained invariant for both models.

Models 1 and 2 for the structures of **1** and **2** were tested by electronic-structure calculations with the notion that the configuration with the lowest total energy is the correct one. For **1**, model 2 proved to be more stable in energy than model 1 by a substantial amount of about 3 eV per formula unit.[40] This result was consistent with the X-ray refinement data pointing to the validity of the Ga/Ge assignment according to model 2. This particular assignment was therefore chosen for the structure of **1**.

In the case of **2**, theoretical structure calculations showed that model 2 is also more stable than model 1, by 0.15 eV per formula unit.[40] This is in accord with the results obtained for **1**. However, by choosing configuration 1 for **2**, the Yb–M bond of 3.0072(17) Å had to be assigned as Yb–Ga, whereas such connectivity is more typical for Yb–Ge.

Table 4. Selected bond lengths [Å] for $Yb_2Ga_4Ge_6$ (**1**).

Bond	Distance	Mult.	Bond	Distance	Mult.
Yb(1)–Ge(1)	3.0774(14)	×1	Ge(1)–Ga(2)	2.5050(18)	×1
Yb(1)–Ga(4)	3.0957(15)	×1	Ge(1)–Ge(5)	2.5081(11)	×2
Yb(1)–Ge(2)	3.1273(11)	×2	Ge(1)–Ga(1)	2.547(2)	×1
Yb(1)–Ge(3)	3.1726(15)	×1	Ge(2)–Ga(4)	2.5340(12)	×2
Yb(1)–Ge(5)	3.1884(11)	×2	Ge(2)–Ge(5)	2.5713(19)	×1
Yb(1)–Ge(3)	3.2106(15)	×1	Ge(2)–Ga(3)	2.5863(19)	×1
Yb(1)–Ga(2)	3.3202(15)	×1	Ge(3)–Ga(2)	2.4666(18)	×1
Yb(1)–Ga(3)	3.3836(13)	×2	Ge(3)–Ga(3)	2.4849(10)	×2
Yb(1)–Ga(3)	3.4982(13)	×2	Ge(3)–Ga(4)	2.577(2)	×1
Yb(2)–Ge(5)	3.0567(14)	×1	Ge(4)–Ga(1)	2.4658(12)	×2
Yb(2)–Ge(6)	3.0616(10)	×2	Ge(4)–Ga(4)	2.5271(19)	×1
Yb(2)–Ge(4)	3.0833(11)	×2	Ge(4)–Ge(6)	2.5672(19)	×1
Yb(2)–Ge(2)	3.1200(15)	×1	Ge(5)–Ga(3)	2.5326(19)	×1
Yb(2)–Ga(1)	3.1231(13)	×2	Ge(6)–Ga(2)	2.4745(10)	×2
Yb(2)–Ge(1)	3.3445(11)	×2	Ge(6)–Ga(1)	2.505(2)	×1
Yb(2)–Ga(4)	3.4882(13)	×2			

Table 5. Atomic coordinates and equivalent isotropic displacement parameters[a] [$Å^2 \times 10^3$] for $RE_3Ga_4Ge_6$ (**2**; RE = Yb, Eu).

Atomic position	Wyckoff symbol	*x*	*y*	*z*	*U*(eq)
Yb(1)	4c	0.1759(1)	0	0.5475(1)	13(1)
Eu(1)		0.1743(1)		0.5447(1)	7(1)
Yb(2)	4c	0.4764(1)	0	0.1682(1)	10(1)
Eu(2)		0.4770(1)		0.1691(1)	6(1)
Yb(3)	4c	0.6447(1)	0	0.1063(1)	10(1)
Eu(3)		0.6447(1)		0.1018(1)	6(1)
Ge(1)	4c	0.0225(1)	0	0.6040(2)	12(1)
		0.0235(1)		0.6021(1)	6(1)
Ge(2)	4c	0.2254(1)	0	0.0262(1)	10(1)
		0.2661(1)		0.0251(1)	6(1)
Ge(3)	4c	0.2917(1)	0	0.6416(1)	9(1)
		0.2991(1)		0.6443(2)	7(1)
Ge(4)	4c	0.3478(1)	0	0.2359(1)	9(1)
		0.3480(1)		0.2378(1)	6(1)
Ge(5)	4c	0.6040(1)	0	0.3662(1)	12(1)
		0.6049(1)		0.3639(1)	6(1)
Ge(6)	4c	0.0515(1)	0	0.0340(1)	11(1)
		0.0515(1)		0.0355(1)	6(1)
Ga(1)	4c	0.4210(1)	0	0.4124(1)	8(1)
		0.4230(1)		0.4172(1)	5(1)
Ga(2)	4c	0.2408(1)	0	0.2572(2)	11(1)
		0.2408(1)		0.2550(2)	6(1)
Ga(3)	4c	0.0652(1)	0	0.2674(2)	10(1)
		0.0658(1)		0.2742(2)	6(1)
Ga(4)	4c	0.8644(1)	0	0.1146(1)	10(1)
		0.8623(1)		0.1193(2)	7(1)

[a] *U*(eq) is defined as one-third of the trace of the orthogonalized U^{ij} tensor.

Hence, further tests of modified configuration 2 were carried out. In subsequent electronic-structure calculations, the Ga atom located 3.0072(17) Å from Yb was switched to a Ge atom, to conform to the original assignment requiring shorter Yb–Ge distances. However, in order to keep the number of electrons constant, one of the Ge sites had to be switched to Ga. Consequently, the Ge atom at the trigonal planar site was chosen, as the corresponding Yb–M distances allowed. Interestingly, the resulting structure was the least stable in energy and was higher than configuration 2 by 0.86 eV per formula unit.[40] Thus, the original configuration 2 was chosen in the case of **2** as well, and it is reported

Table 6. Selected bond lengths [Å] for $Yb_3Ga_4Ge_6$ (**2**).

Bond	Distance	Mult.	Bond	Distance	Mult.
Yb(1)–Ge(3)	2.9321(17)	×1	Yb(3)–Ga(3)	3.3579(14)	×2
Yb(1)–Ge(3)	3.0563(13)	×2	Yb(3)–Ge(2)	3.4618(18)	×1
Yb(1)–Ga(1)	3.1654(13)	×2	Yb(3)–Ga(2)	3.4949(15)	×1
Yb(1)–Ge(4)	3.2213(13)	×2	Ge(1)–Ge(1)	2.490(3)	×1
Yb(1)–Ge(5)	3.3323(14)	×2	Ge(1)–Ga(1)	2.5036(13)	×2
Yb(1)–Ga(2)	3.564(2)	×1	Ge(1)–Ga(3)	2.555(2)	×1
Yb(1)–Ga(2)	3.5650(15)	×2	Ge(2)–Ge(2)	2.4775(16)	×2
Yb(2)–Ga(1)	3.0072(17)	×1	Ge(2)–Ga(2)	2.540(2)	×1
Yb(2)–Ge(6)	3.1046(13)	×2	Ge(2)–Ga(4)	2.611(2)	×1
Yb(2)–Ge(6)	3.1479(13)	×2	Ge(3)–Ge(5)	2.501(2)	×1
Yb(2)–Ga(3)	3.1587(14)	×2	Ge(3)–Ga(2)	2.5020(13)	×2
Yb(2)–Ge(4)	3.1838(18)	×1	Ge(4)–Ga(4)	2.5165(13)	×2
Yb(2)–Ge(1)	3.2521(15)	×2	Ge(4)–Ga(1)	2.573(2)	×1
Yb(2)–Ga(4)	3.4427(15)	×2	Ge(4)–Ga(2)	2.579(2)	×1
Yb(3)–Ge(2)	2.9970(12)	×2	Ge(5)–Ga(1)	2.504(2)	×1
Yb(3)–Ge(5)	3.0232(18)	×1	Ge(5)–Ga(3)	2.5241(13)	×2
Yb(3)–Ge(3)	3.1125(17)	×1	Ge(6)–Ge(6)	2.558(3)	×1
Yb(3)–Ge(6)	3.1475(13)	×2	Ge(6)–Ga(3)	2.562(2)	×1
Yb(3)–Ga(4)	3.1985(14)	×2	Ge(6)–Ga(4)	2.617(2)	×1

below. For both structures **1** and **2**, the determined Ga/Ge distribution was later found to be in accordance with the magnetic measurements (see below) and with the Zintl concept of bonding, which further validated the atomic assignment.

Electronic properties and band-structure calculations: To obtain further insight into the bonding and transport properties of **1** and **2**, electronic-structure calculations were carried out. The total densities of states (DOS) for **1** and **2** are shown in Figures 6A and 7A. The calculation predicts both **1** and **2** to be poor metals, with DOS at the Fermi energy E_F of 1.25 states/(eV[$Yb_2Ga_4Ge_6$]) and 6.2 states/(eV[$Yb_3Ga_4Ge_6$]) respectively (see insets to Figures 6A and 7A). The Yb f levels lie very close to E_F and contribute to the DOS at E_F. To find the non-f electron contribution to the DOS at E_F, we also performed calculations on the hypothetical Sr compounds "$Sr_2Ga_4Ge_6$" and "$Sr_3Ga_4Ge_6$", which confirmed that these are semimetals with very low DOS at E_F of 0.26 states/(eV[$Sr_2Ga_4Ge_6$]) and 0.86 states/(eV[$Sr_3Ga_4Ge_6$]), respectively. The semimetallic character arises from the fact that the expected band gap in these compounds is negative, that is, the bottom of the expected conduction band lies in energy below the states at the top of what would be considered to be the valence band. This is seen clearly in spaghetti plots of the band structures (not shown).

The partial DOS analysis for **1** and **2** reveals that the largest contribution to the total DOS in the range from −2 eV to about 0 eV comes from the Yb f levels (Figures 6A and 7A). The two narrow peaks observed are the result of splitting of Yb f states due to spin–orbit interaction. The location of these peaks close to, yet below, E_F suggests that Yb f states are fully occupied. This indicates the f^{14} electron configuration corresponding to Yb^{2+}, consistent with the results of magnetic measurements.

Because partial DOS of all Ga and Ge atoms in **1** and **2** show similar features, two representative atoms (Ga(1),

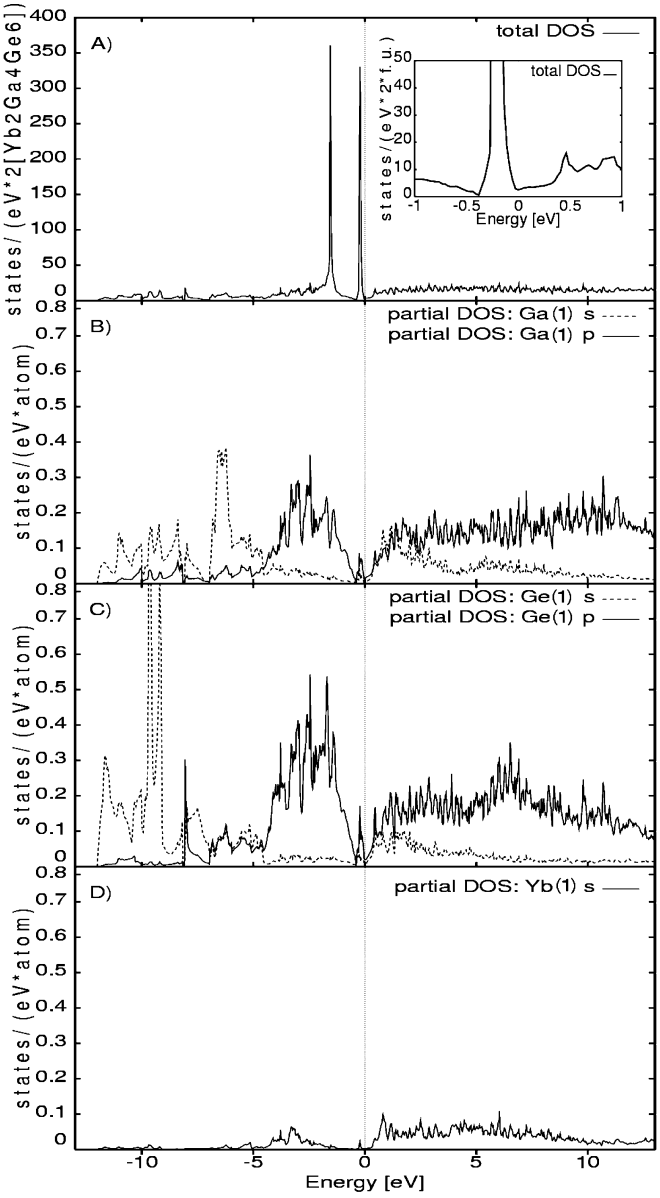

Figure 6. Density of states (DOS) plot for $Yb_2Ga_4Ge_6$ (**1**). The Fermi level E_F is drawn as a dotted line. A) Total DOS (inset: expanded area of DOS near the Fermi level); B) partial DOS arising from Ga(1) s and p states; C) partial DOS from Ge(1) s and p states; D) contribution of Yb(1) s states to DOS.

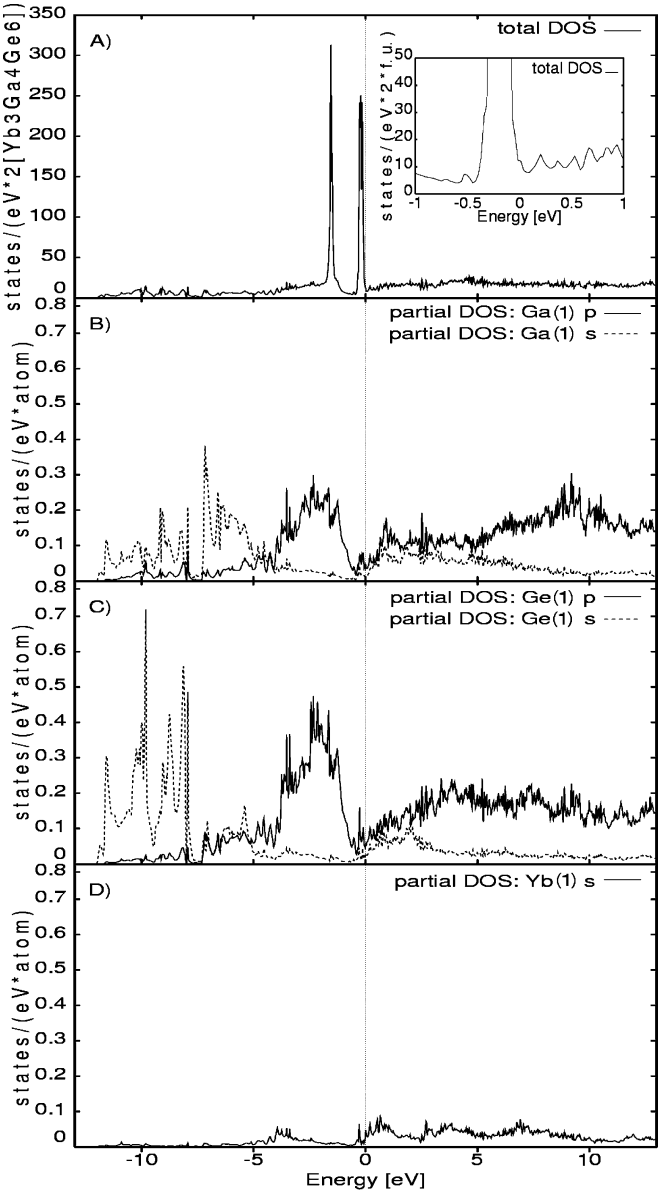

Figure 7. Density of states (DOS) plot for $Yb_3Ga_4Ge_6$ (**2**). The Fermi level E_F is drawn as a dotted line. A) Total DOS (inset: expanded area of DOS near the Fermi level); B) partial DOS arising from Ga(1) s and p states; C) partial DOS from Ge(1) s and p states; D) contribution of Yb(1) s states to DOS.

Ge(1)) were chosen for Ga/Ge partial DOS analysis. The Ga s levels in **1** and **2** range from −12 to −5 eV, and the Ga p levels from −5 to 10 eV, as shown in Figures 6B and 7B. Similarly, the Ge s levels in **1** and **2** mainly lie in the interval between −12 and −5 eV, and for the Ge p levels between −5 and 10 eV (Figures 6C and 7C). As seen from the partial DOS, the Ga p and Ge p states between −5 and 10 eV are highly hybridized, and this suggests a strong covalent interaction within the $[Ga_4Ge_6]$ framework. Indications for strong covalent interaction were already seen in the short Ga–Ge and Ge–Ge distances, as discussed above. Additionally, the Yb s and f states also hybridize with the Ga p and Ge p states, that is, the Yb atoms act not only as electron donors (Yb^{2+}) to the $[Ga_4Ge_6]$ framework, but also participate in covalent bonding with it (Figures 6D and 7D). The observed weak hybridization of Yb and Ga/Ge states further reinforces the idea of covalent bonding between the Yb atoms and the $[Ga_4Ge_6]$ framework.

Considering the above, we expect metallic properties for **1** and **2**, as opposed to the semiconducting behavior characteristic for classical Zintl phases. As has been noted by a number of researchers, the predicted semiconducting behavior has only been seen in relatively few "closed-shell" Zintl compounds.[41] In many cases the observed properties are in fact metallic. The question whether this phenomenon is caused by adventitious doping with impurities or incomplete charge transfer from the electropositive cation species to the host framework is still open.[10]

Physical properties

Magnetism: The plots of the molar susceptibility χ_m of crystalline samples of **1** and **2** (RE = Yb) as a function of temperature are presented in Figure 8. Compounds **1** and **2** have very low susceptibilities, which are nearly independent

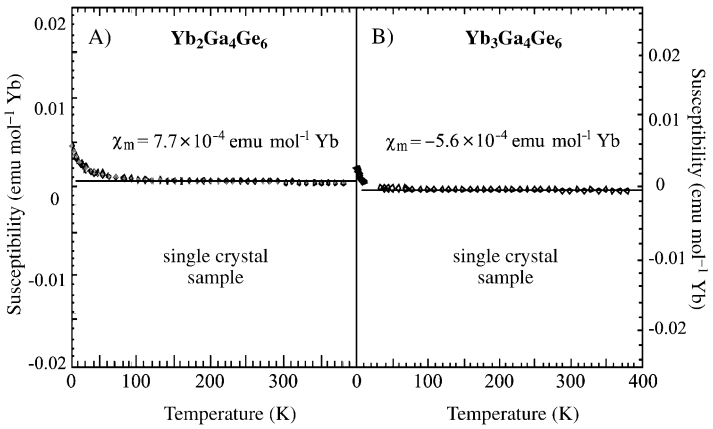

Figure 8. Temperature dependence of the magnetic susceptibility of crystalline samples of A) $Yb_2Ga_4Ge_6$ (**1**) and B) $Yb_3Ga_4Ge_6$ (**2**) calculated per mole of Yb.

of temperature (Figure 8). The small upturn of χ_m at low temperatures may be due to the presence of paramagnetic impurities. The temperature-independent behavior of χ_m for **1** and **2** (RE = Yb) implies a nonmagnetic state for the Yb ions and a completely filled f configuration (Yb^{2+}). The positive sign of χ_m in **1** is indicative of Pauli paramagnetism.

In contrast to **1**, the magnetic response of **2** is diamagnetic (χ_m is negative). Therefore, it follows that in **2** the contribution to the magnetic susceptibility from the core diamagnetism of constituent atoms surpasses the paramagnetic contribution due to the presence of conduction electrons (Pauli paramagnetism). Interestingly, in our previous studies on intermetallic compounds with nonmagnetic RE atoms, we found that systems which exhibit metallic conductivity[42] typically behave as Pauli paramagnets. Examples include $Y_{0.67}Ni_2Ga_{5-x}Ge_x$ ($+0.13\cdot10^{-3}$ emu (mol Y)$^{-1}$),[4] $Y_{0.67}Co_2Ga_{6-x}Ge_x$ ($+0.11\cdot10^{-3}$ emu (mol Y)$^{-1}$),[4] $La_{5-x}Ni_{12}Sn_{24}$ ($+2.83\cdot10^{-3}$ emu (mol La)$^{-1}$),[43] and $YCoGa_3Ge$ ($+0.6\cdot10^{-3}$ emu (mol Y)$^{-1}$).[6]

The Eu analogue of **2** displays paramagnetic behavior at higher temperatures with a transition to an antiferromagnetic state at 10 K. Above 10 K, the temperature dependence of the reciprocal susceptibility obeys the Curie–Weiss law with an effective magnetic moment of about 7.30 μ_B and a Weiss constant of 5.7 K. The calculated effective magnetic moment for free Eu^{2+} is predicted to be equal to the value of a Gd^{3+} (f^7) ion, that is, 7.94 μ_B.[44] This value is in fair agreement with the experimental value found for $Eu_3Ga_4Ge_6$ and is thus indicative of the presence of Eu^{2+} ions in this compound. Recently, the Zintl compound $Eu_4Ga_8Ge_{16}$ was shown by Mössbauer spectroscopy to contain Eu^{2+} ions, and the susceptibility measurements found that this compound follows the Curie–Weiss law with an effective magnetic moment of 8.0 μ_B.[45]

Transport properties: For **1** and **2**, the X-ray structural data and theoretical electronic calculations seem to suggest poor metallic behavior, which is supported by the electrical conductivity data. In particular, the observed charge-transport properties are consistent with the notion of strong covalent bonding between the Yb atom and the $[Ga_4Ge_6]^{n-}$ network. Nevertheless, the possibility of overdoping (for example caused by slight deviations from the ideal stoichiometric Ga/Ge ratio) cannot be ruled out.

Electrical conductivity and thermopower measurements were performed on single-crystal samples of $Yb_3Ga_4Ge_6$ (**2**). The almost linear decrease in conductivity with increasing temperature indicates metallic behavior (Figure 9A). The

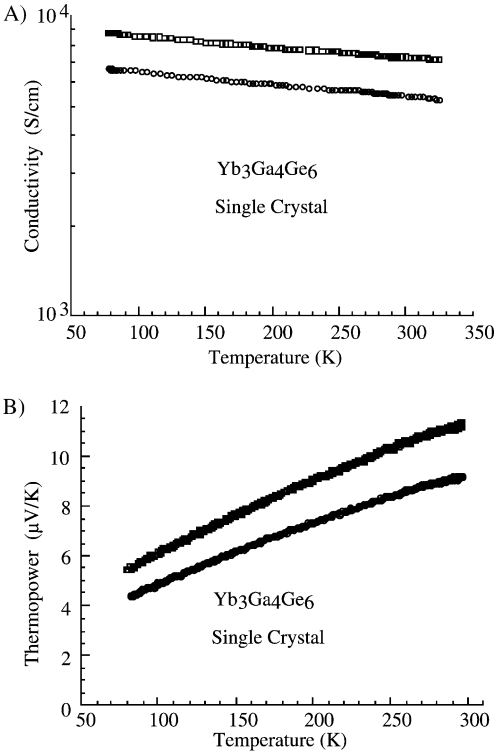

Figure 9. Transport properties of $Yb_3Ga_4Ge_6$ (**2**) as a function of temperature. A) Electrical conductivity (four-probe) and B) thermopower. Data from two different single-crystal samples are shown.

room-temperature value of about 7000 S cm^{-1} is typical of relatively poor metals. The temperature dependence of the thermoelectric power between 80 and 300 K is shown in Figure 9B. The thermopower is small, consistent with the metallic nature of the material, and the positive values (ca. 10 μV K^{-1}) signify that the charge carriers are holes, .

Conclusion

The new compounds $Yb_2Ga_4Ge_6$ and $Yb_3Ga_4Ge_6$ were grown from solutions in molten Ga; the latter also has a eu-

ropium analogue. The structure and bonding of these compounds was described within the Zintl bonding concept. Bonding considerations based on this concept in conjunction with electronic-structure calculations allowed the assessment of the Ga/Ge distribution in their structures. The pair of compounds described here provides an excellent illustration of the validity and power of the Zintl concept, because it can rationalize very nicely how a difference of two electrons can influence the framework bonding. In contrast to more classical Zintl compounds with alkali and alkaline-earth metals, in which the metal atoms act strictly as electron donors, the electropositive divalent RE atoms in the present compounds bind strongly to the polyanionic $[Ga_4Ge_6]^{n-}$ framework, which is a three-dimensional rigid unit held together by strong Ga–Ge and Ge–Ge interactions. Calculations of the theoretical band structure predict these materials to have metallic properties, a fact verified experimentally for $Yb_3Ga_4Ge_6$.

In the traditional understanding, Zintl phases are semiconductors; however, the present and previous investigations show that they can also be metals. In the case of metallic Zintl compounds, all valence electrons can still be formally assigned to the polyanionic part, the bonding of which should follow valence rules for localized bonding. Nevertheless, the metallic as opposed to semiconducting behavior of $Yb_2Ga_4Ge_6$ and $RE_3Ga_4Ge_6$ can be understood as the result of strong covalent interactions of the electrons of the Yb atom with the framework, which results in a dramatic narrowing of the band gap to zero and even to negative values.

Experimental Section

Flux synthesis: To prepare $Yb_2Ga_4Ge_6$ (**1**) and $Yb_3Ga_4Ge_6$ (**2**), elemental Yb, Ga, and Ge of typical purity 99.9% or higher (Cerac Inc.) were combined in the molar ratios 1:15:3 (Yb 0.695 mmol, Ga 10.5 mmol, Ge 2.09 mmol) and 1:10:2 (Yb 0.985 mmol, Ga 9.85 mmol, Ge 1.97 mmol), respectively, and placed in alumina crucibles. The metals were handled in a glove box under nitrogen atmosphere. The crucibles were then sealed in silica ampoules under vacuum (ca. 10^{-4} Torr). For **1**, the reaction mixture was heated to 800°C over 10 h, held at 800°C for 36 h, and then cooled to 200°C over 18 h. For **2** ($Yb_3Ga_4Ge_6$), the reaction mixture was heated to 1000°C over 15 h, kept at 1000°C for 5 h, then cooled to 850°C, kept at this temperature for three days, and finally cooled to 200°C at a rate of 18°C h^{-1}. On completion of the reactions, most of the unused flux was removed by filtration at about 200°C through a specially designed silica filter with a coarse frit. Further isolation was done in a 3–5 M solution of iodine in DMF over 24 h at room temperature. The product was rinsed with DMF and water, and dried with acetone and diethyl ether. From these reactions, crystals of monoclinic $Yb_3Ga_4Ge_6$ and orthorhombic $Yb_2Ga_4Ge_6$ phases were recovered in about 100% yield. The crystals of **1** and **2** have characteristic dark gray color and metallic luster. The size of the flux-grown crystals reaches a few millimeters in one dimension.

Direct combination: $RE_3Ga_4Ge_6$ (**2**; RE = Yb, Eu) was originally isolated from a reaction of equimolar ratios of these elements. For the rational synthesis of **2**, 1 mmol of RE (99.9%, 5–10 mm ribbons, Cerac), 1.25 mmol Ga (99.99%, 2–5 mm shot, Cerac), and 2.0 mmol Ge (99.999%, −50 mesh, Plasmaterials) were combined in a graphite crucible, which was then flame-sealed under a reduced atmosphere of 10^{-4} Torr in a fused-silica tube. The reactants were heated to 900°C over 10 h. This temperature was maintained for 24 h followed by slow cooling to room temperature over 48 h. The resulting product was composed of 70% large silver pieces (target phase) and 30% of loose black powder (side product).

Elemental analysis and X-ray powder diffraction: The elemental composition of grown crystals was determined by energy dispersive spectroscopy (EDS) on a SEM JEOL JSM-35C scanning electron microscope equipped with a NORAN Inc. EDS detector. Data were acquired at an acceleration voltage of 20 kV and a collection time of 30 s. Extensive averaging of results obtained on different crystals was carried out. Additionally, the freshly exposed surfaces of cross-sectioned crystals were analyzed to check for errors due to possible contamination with surface-adhering impurities. The EDS results obtained from the surface and cross-sectioned areas were then compared. The average compositions (normalized to the amount of Yb(Eu)) were determined to be $Yb_2Ga_{4.3}Ge_{5.1}$ and $Yb_3Ga_{4.2}Ge_{4.7}$ ($Eu_3Ga_{3.3}Ge_{5.6}$) for **1** and **2**, respectively. This is in agreement with the single-crystal X-ray refinement, which led to the formulas $Yb_2Ga_4Ge_6$ and $Yb_3Ga_4Ge_6$ ($Eu_3Ga_4Ge_6$).

The X-ray powder diffraction (XRD) patterns of products were recorded at room temperature on a CPS 120 INEL X-ray diffractometer ($Cu_{K\alpha}$ radiation) equipped with a position-sensitive detector. Experimental XRD patterns were compared to those calculated from single-crystal data using the CERIUS^2 software package.[46]

Single-crystal X-ray diffraction: The intensity data were collected on single crystals of **1** ($Yb_2Ga_4Ge_6$) and **2** ($Yb_3Ga_4Ge_6$, $Eu_3Ga_4Ge_6$) at room temperature with a Siemens Platform SMART[47] CCD X-ray diffractometer. For **1**, a crystal of suitable size ($0.12\times0.10\times0.08$ mm) was cut from a larger crystal and mounted on a glass fiber. Needlelike single crystals of $Yb_3Ga_4Ge_6$ and $Eu_3Ga_4Ge_6$ with dimensions of $0.06\times0.08\times0.30$ mm and $1.1\times0.05\times0.05$ mm, respectively, were selected for data collection of **2**. A full sphere of reflections ($Mo_{K\alpha}$ radiation, $\lambda = 0.71073$ Å) was acquired up to 60° in 2θ. The individual frames were measured with ω steps of 0.30° and an exposure time of 20–30 s per frame. The data acquisition and cell reduction was done with SMART,[47] and data reduction was performed with the SAINTPLUS[48] software package. The face-indexing routine was next applied for analytical absorption corrections. An empirical correction for absorption based on symmetry-equivalent reflections was applied with the SADABS program. The structures were solved and refined by direct methods with the SHELXTL software package. All atomic positions were refined anisotropically. The setting of the cell was standardized with the STRUCTURE TIDY program.[49]

Physical properties: A conventional four-probe method and a slow ac technique were used for electrical conductivity and thermopower measurements[50] in the temperature range of 4–300 K.

Single-crystal and polycrystalline samples of **1** ($Yb_2Ga_4Ge_6$) and **2** ($RE_3Ga_4Ge_6$, RE = Yb, Eu) were used for the magnetic measurements, which were performed on a MPMS SQUID magnetometer (Quantum Design, Inc.) in the temperature range 2–400 K with an external applied magnetic field of 10000 G for **1** and 500 G for **2**. The magnetization data were corrected for sample-holder contribution and for core diamagnetism in the case of $Eu_3Ga_4Ge_6$.

Differential thermal analysis (DTA) was carried out on polycrystalline samples of **1** and **2** to determine melting points of these two phases, as well as to test for phase changes such as a possible interconversion of **1** and **2**. The analysis was performed with a Shimatzu DTA-50 differential thermal analyzer with α-Al_2O_3 as the standard reference.

Methods of calculation: Electronic-structure calculations were performed on $Yb_2Ga_4Ge_6$ and $Yb_3Ga_4Ge_6$, as well as hypothetical compounds "$Sr_2Ga_4Ge_6$" and "$Sr_3Ga_4Ge_6$" by using the self-consistent full-potential linearized augmented plane wave method[51] (LAPW) within density functional theory[52] (DFT). The generalized gradient approximation (GGA) of Perdew, Burke, and Ernzerhof[53] was used for the exchange and correlation potential. The values of the atomic radii were taken to be 2.3 a.u. for Ga and Ge atoms, and 2.5 a.u. for Yb and Sr atoms, where a.u. is the atomic unit (0.529 Å). Convergence of the self-consistent iterations was performed for 21 k points inside the reduced Brillouin zone to within 0.0001 Ry with a cutoff of −6.0 Ry between the valence and the core states. Scalar relativistic corrections were included, and spin–orbit interaction was incorporated by using a second variational procedure.[54] A further relativistic correction of the p states, the $p_{1/2}$ correction[51,55] was included by addition to the second variational basis (scalar-relativistic by construction) of the full-relativistic local orbitals corresponding to

$l=1$ and $j=1/2$ ($p_{1/2}$ local orbitals). The calculations were performed with the WIEN2K program.[56]

Further details of the crystal structure investigations may be obtained from the Fachinformationszentrum Karlsruhe, 76344 Eggenstein-Leopoldshafen, Germany (fax: (+49) 7247-808-666; e-mail: crysdata@fiz-karlsruhe.de) on quoting CSD-413534 ($Eu_3Ga_4Ge_6$), CSD-413535 ($Yb_2Ga_4Ge_6$), and CSD-413536 ($Yb_3Ga_4Ge_6$).

Acknowledgments

Financial support from the Department of Energy (Grant # DE-FG02-99ER45793) is gratefully acknowledged. This work made use of the SEM facilities of the Center for Advanced Microscopy at Michigan State University.

[1] X. Z. Chen, P. Larson, S. Sportouch, P. Brazis, S. D. Mahanti, C. R. Kannewurf, M. G. Kanatzidis, *Chem. Mater.* **1999**, *11*, 75–83.
[2] X. Z. Chen, P. Small, S. Sportouch, M. Zhuravleva, P. Brazis, C. R. Kannewurf, M. G. Kanatzidis, *Chem. Mater.* **2000**, *12*, 2520–2522.
[3] M. A. Zhuravleva, X. Wang, A. J. Schultz, T. Bakas, M. G. Kanatzidis, *Inorg. Chem.* **2002**, *41*, 6056–6061.
[4] M. A. Zhuravleva, X. Z. Chen, X. Wang, A. J. Schultz, J. Ireland, C. K. Kannewurf, M. G. Kanatzidis, *Chem. Mater.* **2002**, *14*, 3066–3081.
[5] M. A. Zhuravleva, M. G. Kanatzidis, *J. Solid State Chem.* **2002**, *173*, 280–292.
[6] M. A. Zhuravleva, R. J. Pcionek, X. Wang, A. J. Schultz M. G. Kanatzidis, *Inorg. Chem.* **2003**, *42*, 6412–6424.
[7] M. A. Zhuravleva, M. Evain, V. Petricek, M. G. Kanatzidis, unpublished results.
[8] D. Bryan, G. D. Stucky, patent pending, **1999**.
[9] A. Bentien, A. Palmqvist, D. Bryan, S. Latturner, G. D. Stucky, L. Furenlid, B. Iversen, *Angew. Chem.* **2000**, *112*, 3759–3762; *Angew. Chem. Int. Ed.* **2000**, *39*, 3613–3616.
[10] D. Bryan, G. D. Stucky, *Chem. Mater.* **2001**, *13*, 252–257.
[11] J. Y. Chan, M. M. Olmstead, S. M. Kauzlarich, D. J. Webb, *Chem. Mater.* **1998**, *10*, 3583.
[12] I. R. Fisher, S. L. Bud′ko, C. Song, P. Canfield, *Phys. Rev. Lett.* **2000**, *85*, 1120–1123.
[13] a) A. Rehr, S. M. Kauzlarich, *J. Alloys Compd.* **1994**, *207*/208, 424–426; b) J. Y. Chan, S. M. Kauzlarich, P. Klavins, R. N. Shelton, D. J. Webb, *Phys. Rev. B* **1998**, *57*, R8103–R8106; c) J. Y. Chan, M. E. Wang, A. Rehr, S. M. Kauzlarich, D. J. Webb, *Chem. Mater.* **1997**, *9*, 2131–2138; d) A. C. Payne, M. M. Olmstead, S. M. Kauzlarich, D. J. Webb, *Chem. Mater.* **2001**, *13*, 1398–1406.
[14] H. Kim, P. Klavins, S. M. Kauzlarich, *Chem. Mater.* **2002**, *14*, 2308–2316.
[15] G. Cordier, H. Schaefer, M. Stelter, *Z. Anorg. Allg. Chem.* **1984**, *519*, 183–188.
[16] A. Holm, S.-M. Park, C. L. Condron, M. M. Olmstead, H. Kim, P. Klavins, F. Grandjean, R. Hermann, G. J. Long, M. G. Kanatzidis, S. M. Kauzlarich, S.-J. Kim, *Inorg. Chem.* **2003**, *42*, 4660–4667.
[17] S.-J. Kim, J. Salvador, D. Bilc, S. D. Mahanti, M. G. , Kanatzidis, *J. Am. Chem. Soc.* **2001**, *123*, 12704–12705.
[18] M. E. Danebrock, C. B. H. Evers, W. Jeitschko, *J. Phys. Chem. Solids* **1996**, *57*, 381–387.
[19] J. Y. Chan, M. M. Olmstead, H. Hope, S. M. Kauzlarich, *J. Solid State Chem.* **2000**, *155* 168–176.
[20] E. A. Leon-Escamilla, W. M. Hurng, E. S. Peterson, J. D. Corbett, *Inorg. Chem.* **1997**, *36*, 703–710.
[21] R. Mishra, R.-D. Hoffman, R. Pöttgen, H. Trill, B. D. Mosel, *Z. Anorg. Allg. Chem.* **2002**, *628*, 741–744.
[22] R. Pöttgen, R.-D. Hoffmann, D. Kussmann, *Z. Anorg. Allg. Chem.* **1998**, *624*, 945–951.
[23] a) E. A. Leon-Escamilla, J. D. Corbett, *Inorg. Chem.* **1999**, *38*, 738–743; b) V. K. Pecharsky, G. D. Samolyuk, V. P. Antropov, A. O. Pecharsky, K. A. Gschneidner, *J. Solid State Chem.* **2003**, *171*, 57–68.
[24] *Chemistry, Structure and Bonding of Zintl Phases and Ions* (Ed.: S. Kauzlarich), VCH, New York, **1996**.
[25] R. Lam, J. Zhang, A. Mar, *J. Solid State Chem.* **2000**, *150*, 371–376.
[26] a) R. Pöttgen, D. Johrendt, *Chem. Mater.* **2000**, *12*, 875–897; b) M. Mizumaki K. Yoshii, H. Kitazawa, H. Tanida, *J. Solid State Chem.* **2003**, *171*, 291–294; c) H. Huppertz, G. Kotzyba, R. D. Hoffmann, R. Pöttgen, *J. Solid State Chem.* **2002**, *169*, 155–159; d) D. Johrendt, G. Kotzyba, H. Trill, B. D. Mosel, H. Eckert, T. Fickenscher, R. Pöttgen, *J. Solid State Chem.* **2002**, *164*, 201–209.
[27] W. Carrillo-Cabrera, S. Paschen, Yu. Grin, *J. Alloys Compd.* **2002**, *333*, 4–12.
[28] J.-G. Mao, J. Goodey, A. Guloy, *Inorg. Chem.* **2002**, *41*, 931–937.
[29] J. R. Salvador, F. Guo, T. Hogan, M. G. Kanatzidis, *Nature* **2003**, *425*, 702.
[30] M. A. Zhuravleva, Doctoral Dissertation Thesis, Michigan State University, **2002**.
[31] Yb_3Ga_9Ge crystallizes in the orthorhombic space group *Cmma*, cell parameters: $a=8.5037(18)$ Å, $b=23.007(4)$ Å, $c=10.786(3)$ Å, $Z=8$, $V=2110.2(9)$ Å^3.
[32] In these reactions Ga is is in excess, as a flux.
[33] The estimated $|E^2-1|$ values for noncentrosymmetric space group is 0.736 and for the centrosymmetric one 0.968.
[34] G. Wulfsberg in *Inorganic Chemistry*, University Science Books, Sausalito, California, **2000**, p. 32.
[35] L. Pauling, *The Nature of the Chemical Bond*, 3rd ed., Cornell University Press, Ithaca, NY, **1960**, p. 410.
[36] The neutron scattering lengths of Ga and Ge atoms differ by about 10%, as opposed to 3% for X-rays.
[37] X. Z. Chen, B. Sieve, R. Henning, A. J. Schultz, P. Brazis, C. R. Kannewurf, J. A. Cowen, R. Crosby, M. G. Kanatzidis, *Angew. Chem.* **1999**, *111*, 695–698; *Angew. Chem. Int. Ed.* **1999**, *38*, 693–696.
[38] B. Sieve, X. Z. Chen, R. Henning, P. Brazis, C. R. Kannewurf, J. A. Cowen, A. J. Schultz, M. G. Kanatzidis, *J. Am. Chem. Soc.* **2001**, *123*, 7040–7047.
[39] For the Eu analogue of **2** ($Eu_3Ga_4Ge_6$), the atomic assignments were based on the results obtained for $Yb_3Ga_4Ge_6$. One reason for more closely studying $Yb_3Ga_4Ge_6$ as opposed to $Eu_3Ga_4Ge_6$ is the ability of DFT calculations to accurately model a filled f level (Yb^{2+}), making accurate calculations of the relative energies of these different atomic-assignment configurations of **2** possible.
[40] The formula unit in this case is $2\times Yb_2Ga_4Ge_6$ for **1** and $2\times Yb_3Ga_4Ge_6$ for **2**.
[41] J. D. Corbett in *Zintl Phases of the Early p-Block Elelments*, (Ed.: S. M. Kauzlarich), VCH, New York, **1996**.
[42] The electrical conductivity was measured for $Y_{0.67}M_2Ga_{5+n-x}Ge_x$, but not for $La_{5-x}Ni_{12}Sn_{24}$ and $YCoGa_3Ge$. However, the latter two do not obey the Zintl–Klemm concept and are expected to be metallic.
[43] M. A. Zhuravleva, D. Bilc, S. D. Mahanti, M. G. Kanatzidis, *Z. Anorg. Allg. Chem.* **2003**, *629*, 327–334.
[44] C. Kittel, *Introduction to Solid State Physics*, 7th Ed., Wiley, New York, **1996**, p. 425.
[45] J. D. Bryan, H. Trill, H. Birkedal, M. Christensen, V. I. Srdanov, H. Eckert, B. B. Iversen, G. D. Stucky, *Phys. Rev. B* **2003**, *68*, art. no. 174429.
[46] CERIUS^2, Version 1.6, Molecular Simulations Inc., Cambridge, England, **1994**.
[47] SMART, Version 5, Siemens Analytical X-ray Systems, Inc., Madison, WI, **1998**.
[48] SAINT, Version 4, Siemens Analytical X-ray Systems, Inc., Madison, WI, **1994–1996**.
[49] L. M. Gelato, E. Parthé, *J. Appl. Crystallogr.* **1987**, *20*, 139–143.
[50] J. W. Lyding, H. O. Marcy, T. J. Marks, C. R. Kannewurf, *IEEE Trans. Instrum. Meas.* **1988**, *37*, 76.
[51] D. Singh, *Planewaves, Pseudopotentials, and the LAPW method*, Kluwer Academic, Boston, **1994**.
[52] a) P. Hohenberg, W. Kohn, *Phys. Rev.* **1964**, *136* B864; b) W. Kohn, L. Sham, *Phys. Rev.* **1965**, *140*, A1133.
[53] J. P. Perdew, K. Burke, M. Ernzerhof, *Phys. Rev. Lett.* **1996**, *77*, 3865.
[54] D. D. Koelling, B. Harmon, *J. Phys. C* **1980**, *13*, 6147.
[55] a) D. D. Koelling, B. Harmon, *J. Phys. C* **1977**, *10*, 3107; b) A. H. MacDonald, W. E. Pickett, D. D. Koelling, *J. Phys. C* **1982**, *13*, 2675; c) P. Novak, unpublished results.

[56] P. Blaha, K. Schwarz, G. Madsen, D. Kvasnicka, J. Luitz, WIEN2K, An Augmented Plane Wave + Local Orbitals Program for Calculating Crystal Properties (Karlheinz Schwarz, Tech. Univ. Wien, Vienna, **2001**).

Received: November 27, 2003

Published online: April 28, 2004

